Egyptian Journal of Petroleum (2016) xxx, xxx–xxx

HOSTED BY

Egyptian Petroleum Research Institute

Egyptian Journal of Petroleum

www.elsevier.com/locate/egyjp
www.sciencedirect.com

FULL LENGTH ARTICLE

Contribution of geophysical studies on detection of the Petrified Frost Qattamiya, Cairo, Egypt

Sultan Awad Sultan Araffa [a], Shokry A. Soliman [b,*], Essam Ghamry [a], Ahmed El Khafif [b], Ahmed Khashba [a], Ahmed S. Soliman [c]

[a] *National Research Institute of Astronomy and Geophysics, 11722 Helwan, Cairo, Egypt*
[b] *Institute of Petroleum Research, Cairo, Egypt*
[c] *Egyptian Environmental Affairs Agency, Egypt*

Received 16 November 2015; revised 15 December 2015; accepted 20 December 2015

KEYWORDS

Geophysical tools;
Petrified wood;
Magnetic;
Resistivity and seismic refraction

Abstract Different geophysical tools such as resistivity, seismic refraction, and magnetic survey have been applied to delineate the subsurface stratigraphy and structural elements, which controlled the distribution and origin of the Petrified wood in Qattamiya, Cairo, Egypt. Land magnetic survey was carried out in the study area through two stages, the first stage includes all area by measuring 11,674 stations and the second stage was carried out in the detailed area that was located at the south-eastern part of the all area including 9441 stations. All measurements have been corrected for diurnal variation and reduced to the north magnetic pole. The results of magnetic interpretation indicated that the area dissected by different structural elements trend toward NE–SW, NW–SE, N–S and E–W directions. Twenty-eight samples have been collected from the detailed area to analyze for magnetic susceptibility values. Four electrical resistivity tomography (ERT) profiles were measured by using dipole–dipole configuration to estimate the vertical and lateral variation of the subsurface sequence. Results of quantitative interpretation of the ERT data indicate that the subsurface sequence consists of different geoelectric units; the first unit is characterized by high resistivity values upto 1000 ohm m corresponding to sand, gravel and Petrified wood at the surface and extends to a depth of a few meters. The second geoelectric unit is corresponding to sandy clay which exhibits moderate resistivity (few hundred ohm m) values with thickness ranging from 6 to10 m. The third geoelectric unit is characterized by very low resistivity corresponding to clay of depth ranging from 10 to 30 m overlaying the fourth unit which reached to a depth ranging from 30 to 56 m and characterized by very high resistivity (8000 ohm m) corresponding to limestone. Three shallow seismic refraction spreads of geophone spacing 7.5 m were measured to investigate the subsurface sequence, where the results of interpretation indicate that the subsurface section consists of three units of average velocity 500, 2000 and 4000 m/s, respectively corresponding to sand, gravel and Petrified wood, sandy clay, clay and limestone.

* Corresponding author.
Peer review under responsibility of Egyptian Petroleum Research Institute.

http://dx.doi.org/10.1016/j.ejpe.2015.12.003

Please cite this article in press as: S.A.S. Araffa et al., Contribution of geophysical studies on detection of the Petrified Frost Qattamiya, Cairo, Egypt, Egypt. J. Petrol. (2016), http://dx.doi.org/10.1016/j.ejpe.2015.12.003

1. Introduction

The area under study "'Petrified Forest" is located in the New Cairo city (Fig. 1a), within the Eastern Desert of Egypt. It lies at about 20 km southeast of Cairo near the Qattamiya region, between longitudes 31° 27′ 30″ and 31° 28′ 30″E and latitudes 29° 58′ 30″ and 29° 59′ 40″N. Topographically, most of the area under consideration is flat. There are a large number of silicified massive tree trunks lying horizontally on the surface or buried partly or completely by sand. The trunks inside the protected area are of Oligocene age and occur above the Maadi Formation, while those overlain by basalt occur outside the protected area [1]. In the Cairo Petrified Forest, the wood physiognomy features of trunks inside and outside the protected area indicate clearly that these trees must have lived in seasonal subtropical or tropical climate; however, this would be the climate of the site of their growth to the east and not necessarily of the site where they are found now [2]. Different geophysical and geologic tools are used for delineating the woods of Petrified Forests such as [3]. They used the electrical resistivity tomography (ERT) and ground penetrating radar for locating buried Petrified wood sites in the natural monument of the Petrified Forest of Evros, Greece. Martz et al. [4] constructed the geologic map of Petrified Forest National Park of Arizona. Refs. [5–8] applied different geophysical techniques in geotechnical and mapping of subsurface structures. The present study aims to delineate the origin wood of the Qattamiya Petrified Forest Protectorate and their trends in the study area.

2. Geology of the study area

The study area is a part of the Cairo-Suez district. The age of different rocks which are exposed in and out of the study area

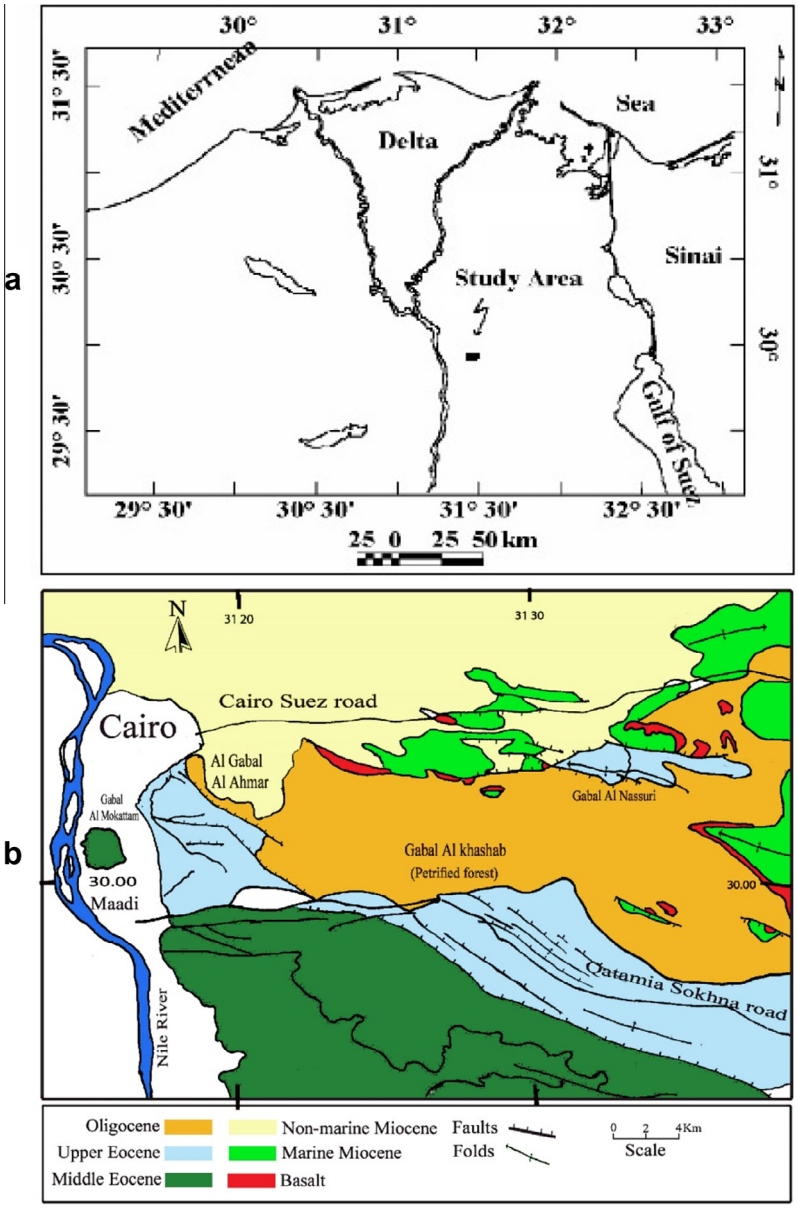

Figure 1 (a) Shows a location map of the study area. (b) Geological map of the area east of Maadi modified after [1].

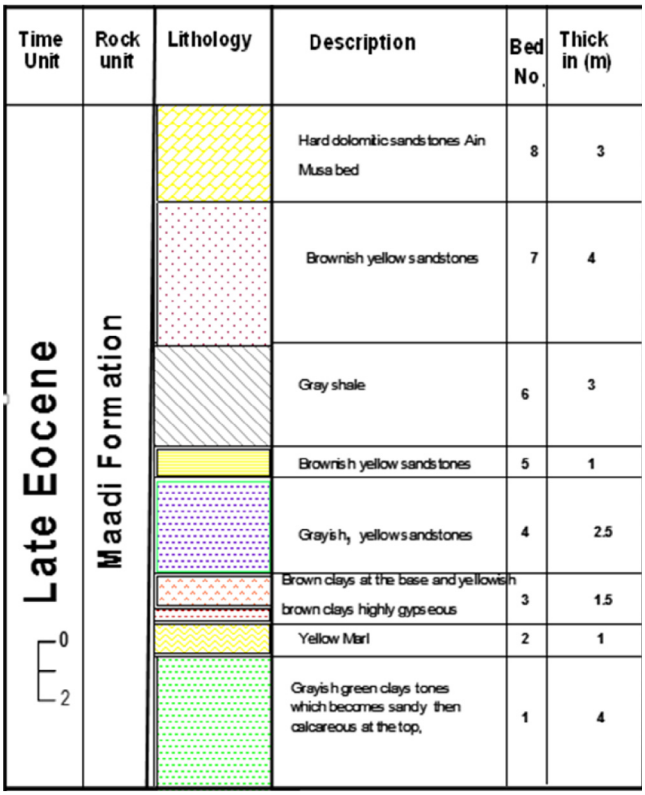

Figure 2 Stratigraphic section of the Late Eocene Maadi Formation at G. El Khashab (Petrified Forest). Modified after [1].

ranges from Upper Eocene to Recent (Fig. 1b). The Upper Eocene is represented in the study area by the Maadi Formation, which consists of intercalated sandy limestone, marl and claystone [9]. In G. El Khashab, the measured thickness of the Maadi Formation is about 21 m. (Fig. 2). It starts at the base by grayish green clays converted to yellowish brown clay in the middle and followed upward by grayish white sandstone, yellow marl with crystalline calcite filling cavities, the intercalation of sandy shale and capped by creamy sandy limestone (Fig. 3). The Maadi Formation unconformably underlies the Oligocene (G. Ahmar Formation or G. El Khashab Formation), and above the Middle Eocene (Guishi Formation). The contact between the Oligocene and the Eocene is recognized by a major unconformity that separates G. El Khashab continental sediments from the underlying marine sediment of the Maadi Formation [10].

The Oligocene deposits in the area seem to be a part of a large graben system which is controlled from the south by the hilly sector of Middle Eocene and from the north by the low land of the Miocene sediments (Fig. 4). The Oligocene fluviatile sediments are usually preserved in the structurally and topographically low areas, while missing on the crests of the structural and topographical highs. Generally, the Oligocene sediments are mainly composed of loose white sands, varicolored sands and gravels with silicified wood (Fig. 5). The studied Petrified logs display a wide range of colours covering the different shades of white, pale-yellow, red and brown (Fig. 6). The longest log encountered measures 30 m and the largest stump is more than one meter in diameter, no roots have been noted, this supports the belief that the trees have been drifted into their present position and then silicified. Akahane et al. [11] concluded that silicified (Petrified) wood had been formed naturally under various conditions by deposition of tiny silica spheres (opal) within it.

3. Methodology

Different geophysical tools are carried out in the study area such as land magnetic survey, 2-D electric resistivity tomography (ERT), shallow seismic refraction and magnetic susceptibility analysis. The geophysical measurements are carried out through two stages.

3.1. First stage

The first stage includes only magnetic measurements to delineate the structures which dissect all the Petrified Forest area.

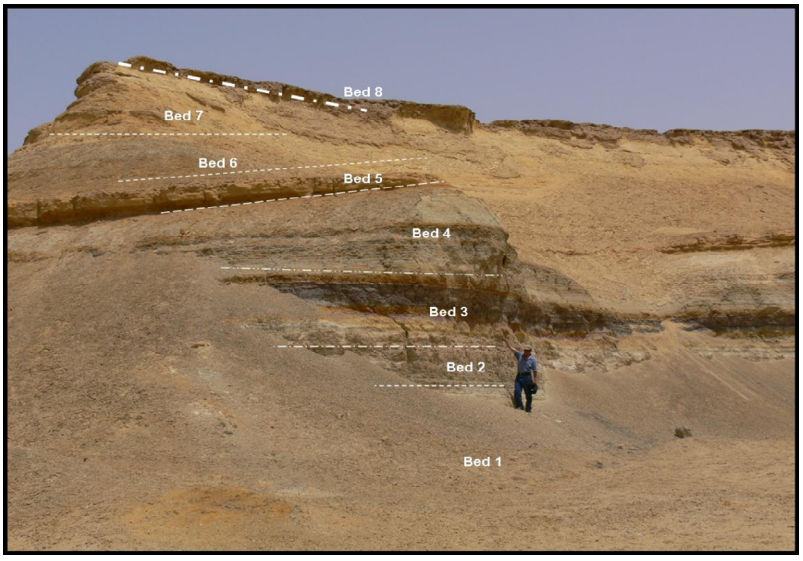

Figure 3 Showing the Maadi Formation at G. El Khashab (Petrified Forest Protectorate).

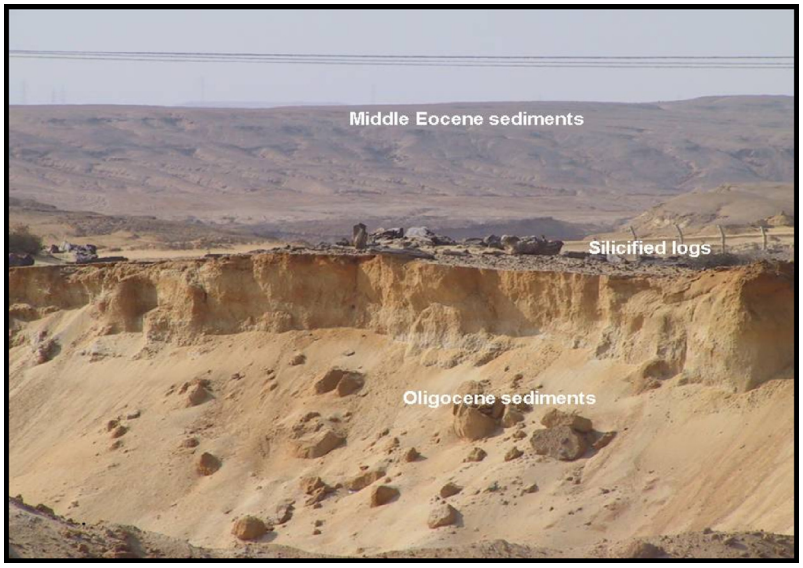

Figure 4 The Oligocene sediments occupying the low land at the Petrified Forest protectorate.

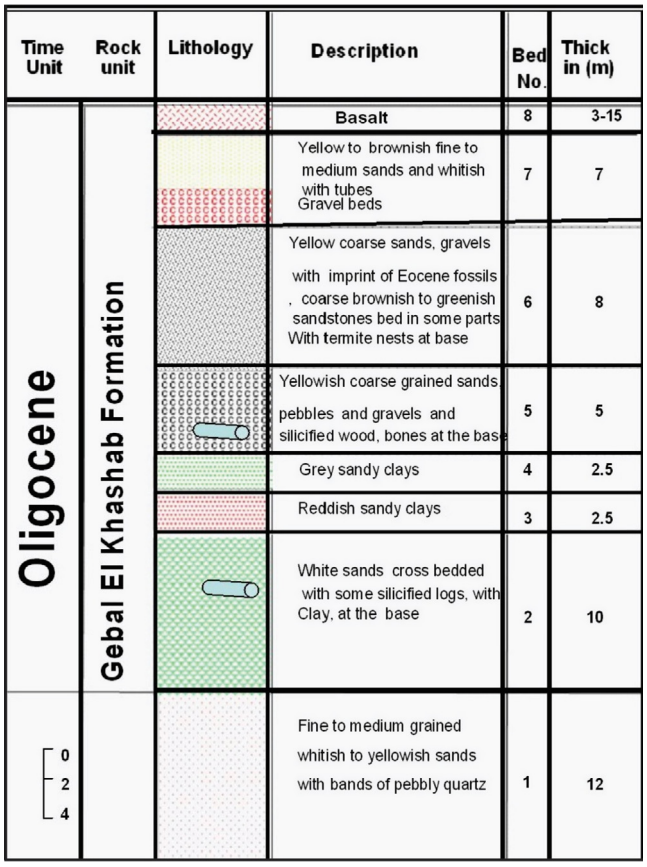

Figure 5 Stratigraphic section of the Oligocene at G. El Khashab. Modified after [1].

3.1.1. Land magnetic survey data acquisition

Eleven thousand and six hundred seventy-four land magnetic stations have been carried out in the study area by using total field magnetometer/gradiometer Overhauser (GSM-19 v7.0) instrument of accuracy ± 0.1 nT covering all the Petrified Forest area (Fig. 7a). The survey was carried out by two types of measurements, the first type is a total intensity magnetic field and the second type is the vertical magnetic gradient. All collected data were corrected for diurnal variation from the recordings of Al Msalat magnetic observatory, the corrected magnetic data plotting by using [12] to represent the total intensity magnetic map (Fig. 7b). The total intensity magnetic map refers to high magnetic anomalies upto 219 nT at the northern part of the area which corresponds to ferruginous sandstone or basaltic flows. The southern part of the area is represented by low magnetic anomalies of 172 nT.

3.1.2. Reduction to the magnetic pole

The magnetic fields created by geological bodies are distorted by the inclination and declination of the earth's field. This can be attributed to the fact that, at low or moderate angles of inclination of the geomagnetic field, the peak of the anomalies has to be shifted away from over the centers of the magnetized bodies, making it difficult to determine correctly the shapes and locations of these magnetized bodies. In order to overcome this distortion in the appearance of an anomaly that depends on its magnetic latitude and the corresponding variation of the dip angle of the magnetization vector in the body a mathematical procedure is adopted on a grid of values of the contour map of the total magnetic intensity. This mathematical procedure was first described by [13–15]. In the present study, the total intensity magnetic map reduced to the pole can be calculated automatically by using [12] of inclination (44.06°), declination (3.28°), magnetic field strength (43143.6 nT) and the height of the instrument sensor from the ground surface is 1 m. A general outlook of the reduced to the magnetic pole map (Fig. 7c) in comparison with the original total intensity magnetic map (Fig. 7b) reflects the northward shift in the positions of the inherited magnetic anomalies due to the elimination of the inclination of the magnetic field in this area. Also, the number of anomalies becomes larger with a comparable decrease of their aerial extension and

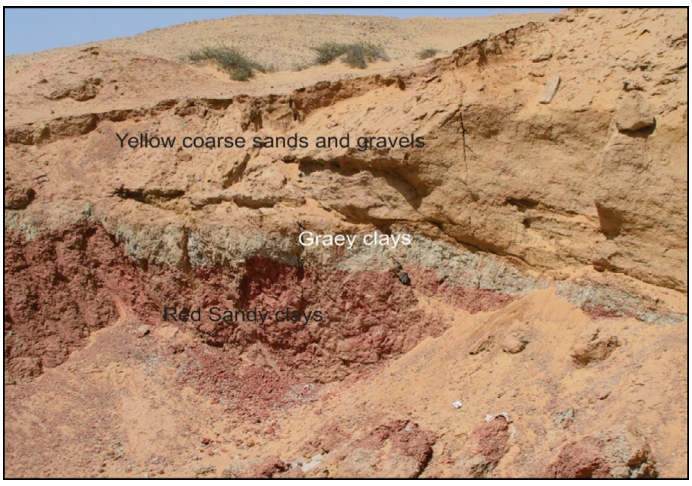

Figure 6 Variegated sequence of reddish and gray clays, east of G. El Khashab area.

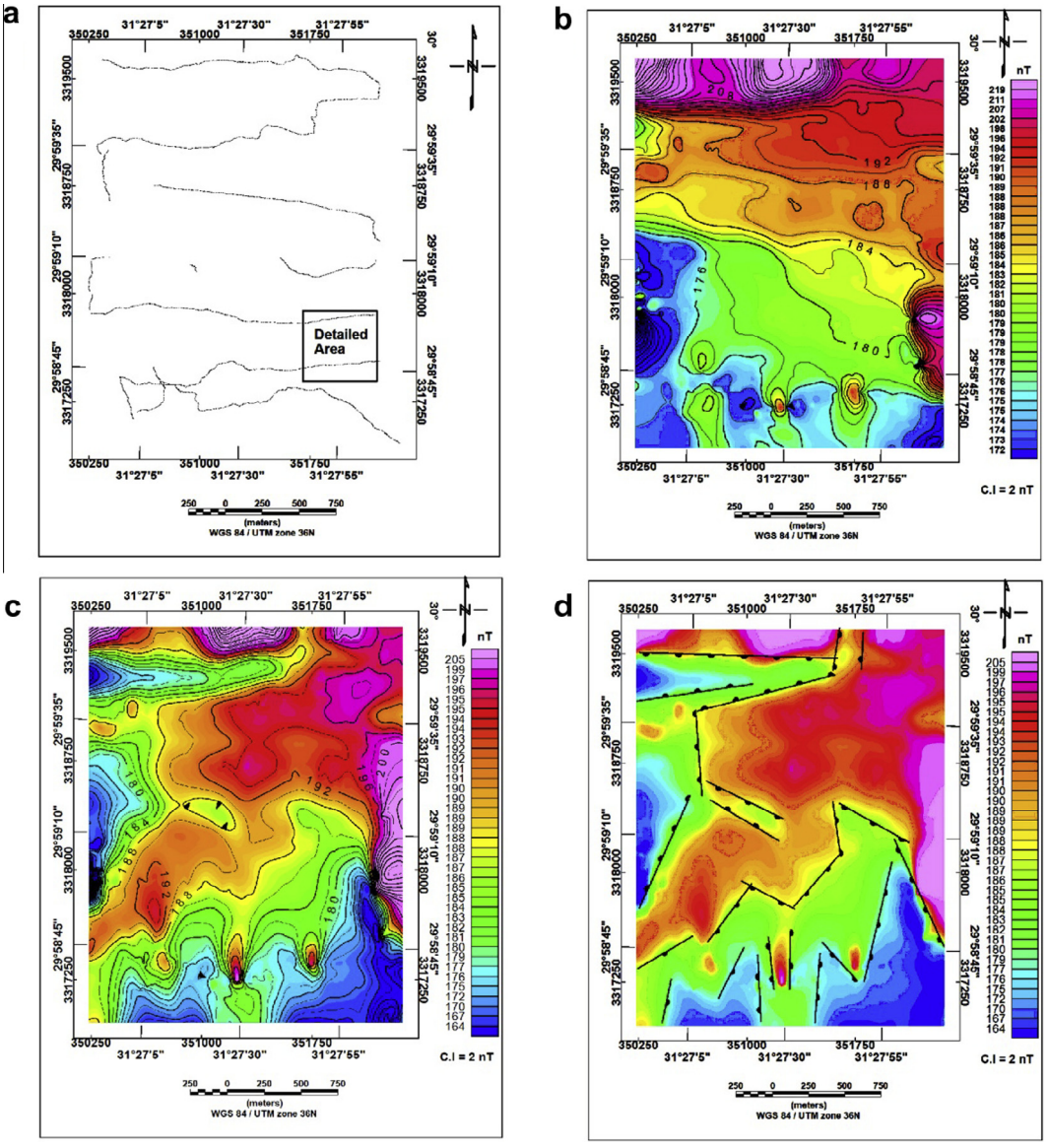

Figure 7 (a) Location of magnetic stations for the first stage. (b) Total intensity magnetic map for the first stage (regional area), (c) total intensity magnetic map, reduced to the pole for the first stage (regional area), (d) fault elements dissecting the regional area.

the increase of their vertical reliefs. The total intensity magnetic map reduced to the pole reflects many fault element trends such as NE–SW, NW–SE, N–S and E–W trends which refer to the trends of Petrified wood as shown from field observations shown in (Fig. 7d). The location of the detailed magnetic area on the RTP map of the regional area indicates that the detailed area is located in the graben area meaning the increasing sedimentary cover in this part.

3.1.3. Depth estimation for magnetic sources

Magnetic data were used to determine the depth of the top of the geologic sources responsible for the observed anomalies. The quantitative interpretation of the total intensity magnetic map was carried out using [12] software. This method is based on the Euler's homogeneity equation. The Euler's homogeneity equation relates the magnetic field and its gradient components to the location of the source, with the degree of homogeneity N, which may be interpreted as a structural index [16]. The structural index is a measure of the rate of change of the field with distance. For example, the magnetic field of a narrow 2D dyke has a structural index of $N = 1$, while a vertical pipe (or cylinder) has $N = 2$. The magnetic field originated by a step and contact has $N = 0$. The suitable structural index seems to be zero (step and contact) represented in (Fig. 8). The solutions obtained using this index for the distribution and the depths of the magnetic sources are compatible with the information collected from the geologic observation. In fact, the depths values obtained for the structures in the southwestern part of the area (varying between 1 and 90 m).

3.1.4. High pass filter

The total intensity magnetic map reduced to the pole (RTP) is used for applying a high pass filter for focusing on the shallow structures and magnetic bodies. The technique of high pass filter was applied by using wave number 2 cycles/km, where the radially average power spectrum (Fig. 9a) refers to the depth of magnetic sources ranging from surface to 0.5 km. The high pass filter map (residual) as shown in (Fig. 9b) indicates that the study area is covered by high magnetic anomalies at the southwestern and central parts. The detailed area still exhibits low magnetic values with respect to a regional area.

3.1.5. Vertical gradient magnetic data

Magnetic data for the first stage were measured also as a magnetic gradient by using magnetometer/gradiometer Overhauser (GSM-19 v7.0) instrument for eleven thousand and six hundred seventy-four stations with the vertical distance between two sensors of 50 cm. Gradient data have been represented by the vertical gradient magnetic map (Fig. 9c). Most of the study area exhibits a high magnetic gradient up to 3 nT and the location of detailed area reflects a low magnetic gradient of about −3.9 nT.

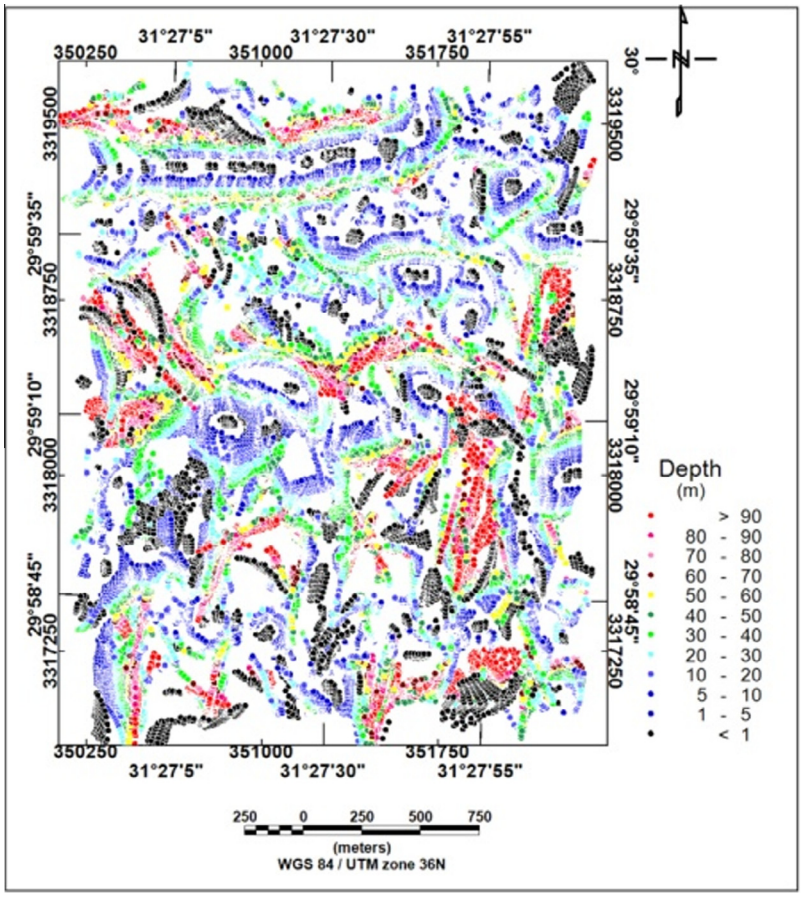

Figure 8 Euler solutions of structural index, =0.0.

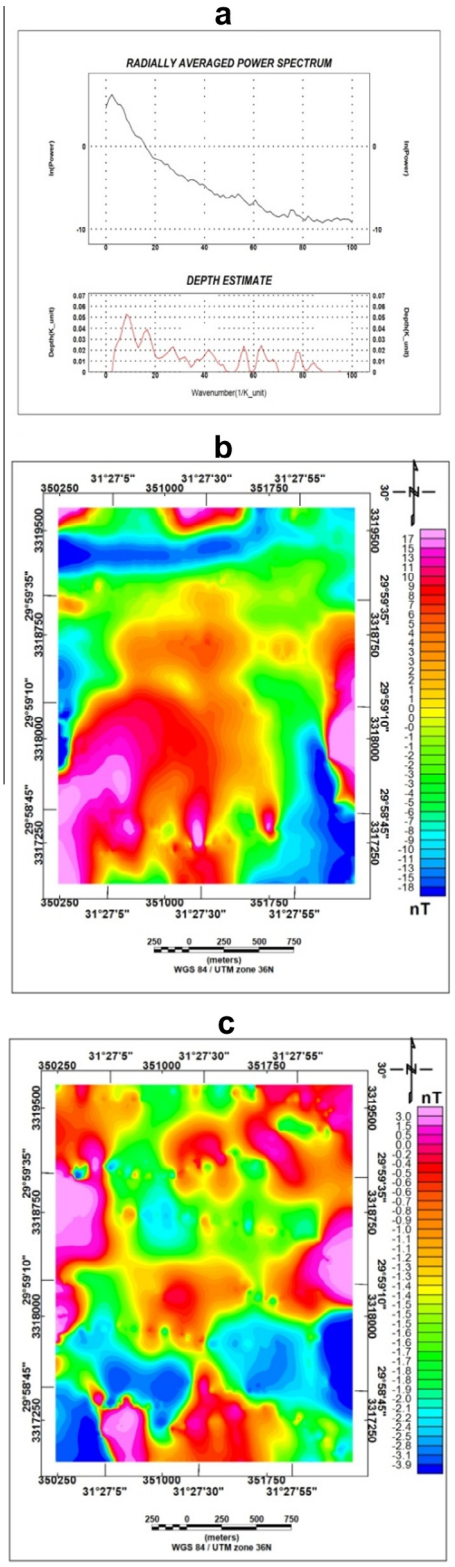

Figure 9 (a) Radially average power spectrum, (b) high pass filter (residual component) of the regional area and (c) vertical gradient magnetic map for the regional area (first stage).

3.2. Second stage (detailed area)

The detailed survey area lies in the southeastern part of the regional area and is located between latitudes 29° 58′ 45″ & 29° 58′ 58″N and longitudes 31° 27′ 15″ & 31° 28′ 05″E which represents an area of 240,000 m squares. The field observation of the regional study area shows that the Petrified wood was traced to the southern part with different trends (detailed area). So different geophysical techniques such as detailed magnetic survey for total intensity and magnetic gradient, electric resistivity tomography (ERT) using the dipole–dipole configuration and shallow seismic refraction data were used to delineate the trends and depths of Petrified wood in the Petrified Forest Protectorate on the Qattamiya area.

3.2.1. Land magnetic survey

Nine thousand four hundred ninety-one magnetic stations were measured by using the same instrument in the first stage (Fig. 10a). The measured data were corrected for diurnal variation from the recordings of Al Msalat magnetic observatory and IGRF to construct the total intensity magnetic map by using [12] are shown in (Fig. 10b). The total intensity magnetic map for the detailed area reflects quite a variation in magnetic field ranging from 168 nT at most of the area to 182 nT at the northeastern part of the study area. The total intensity magnetic map reduced to the magnetic pole using [12] is shown in (Fig. 10c). Also, the detailed area is surveyed by using a vertical magnetic gradient with spacing between two sensors of 50 cm to produce the vertical gradient magnetic map (Fig. 10d). This map indicates variations of the magnetic gradient which varies from high to low according to the variation in magnetic susceptibility which may be related to variation in susceptibility of the Petrified wood. Also, twenty-seven samples were collected from the detailed area for determining the magnetic susceptibility values (Fig. 10e) which are measured by using MS2B Dual Frequency Sensor. The susceptibility map that refers to the eastern part of the study area shows high susceptibility values which are compatible with the RTP map (Fig. 10c) which exhibits high magnetic anomalies at the eastern part of the study area.

3.2.2. Electric resistivity data

Electric resistivity data were collected by using the Syscal-R2 instrument of multi electrode system of 80 electrodes of space 5 m. Four dipole–dipole sections are measured by using electrode spacing (a) 5, 10 and 20 m where the depth of investigation (D) can be calculated from the equation ($D = 1/5$ ($2na$)) where D for "n" number ranging from 1 to 7 to reach a depth of about 56 m (Fig. 11a). The processing and inversion of the dipole–dipole data have been carried out by using RES2DINV software which produces an image of the electrical resistivity distribution in the subsurface based on a regularization algorithm [17]. The inversion model for the four sections indicates that the shallow subsurface section upto 56 m of the study area consists of four essential units. The first unit is composed of sand and Petrified wood at the surface and extends to a depth of a few meters and is

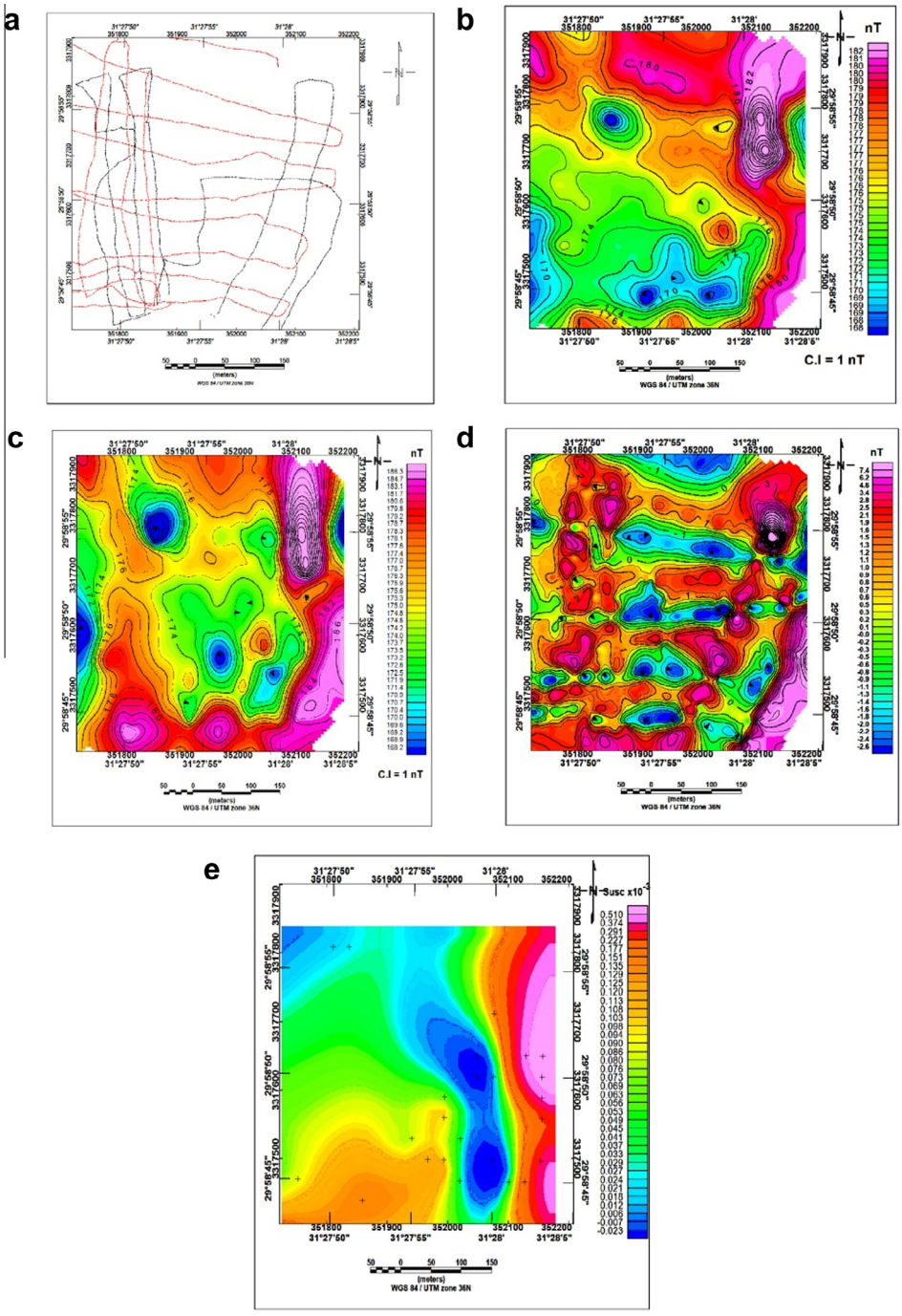

Figure 10 (a) Location map of magnetic survey for detailed area (second stage), (b) total intensity magnetic map, (c) total intensity magnetic map, reduced to the pole, (d) vertical gradient magnetic map, (e) magnetic susceptibility values.

characterized by high resistivity values upto 1000 ohm m. The second unit is composed of sandy clay of moderate resistivity values a few hundred ohm m of thickness ranging from 6 to 10 m. The third unit is composed of clay of low resistivity values of thickness about 20 m and the last units are composed of limestone of very high resistivity up to 8000 ohm m and reached to a depth ranging from 30 to 56 m as shown in (Figs. 11b, c and 12a, b).

3.2.3. Shallow seismic refraction measurements and interpretation

Three P-wave shallow seismic refraction profiles are measured, at the same location of dipole–dipole sections (P1–P3), in the area under investigation (Fig. 11a). We used the McSEIS-SX seismograph (OYO) for data acquisition (24 channels). The length of every profile is 180 m of 7.5 m as a geophone interval and a sledge hammer as seismic sources. The length should be

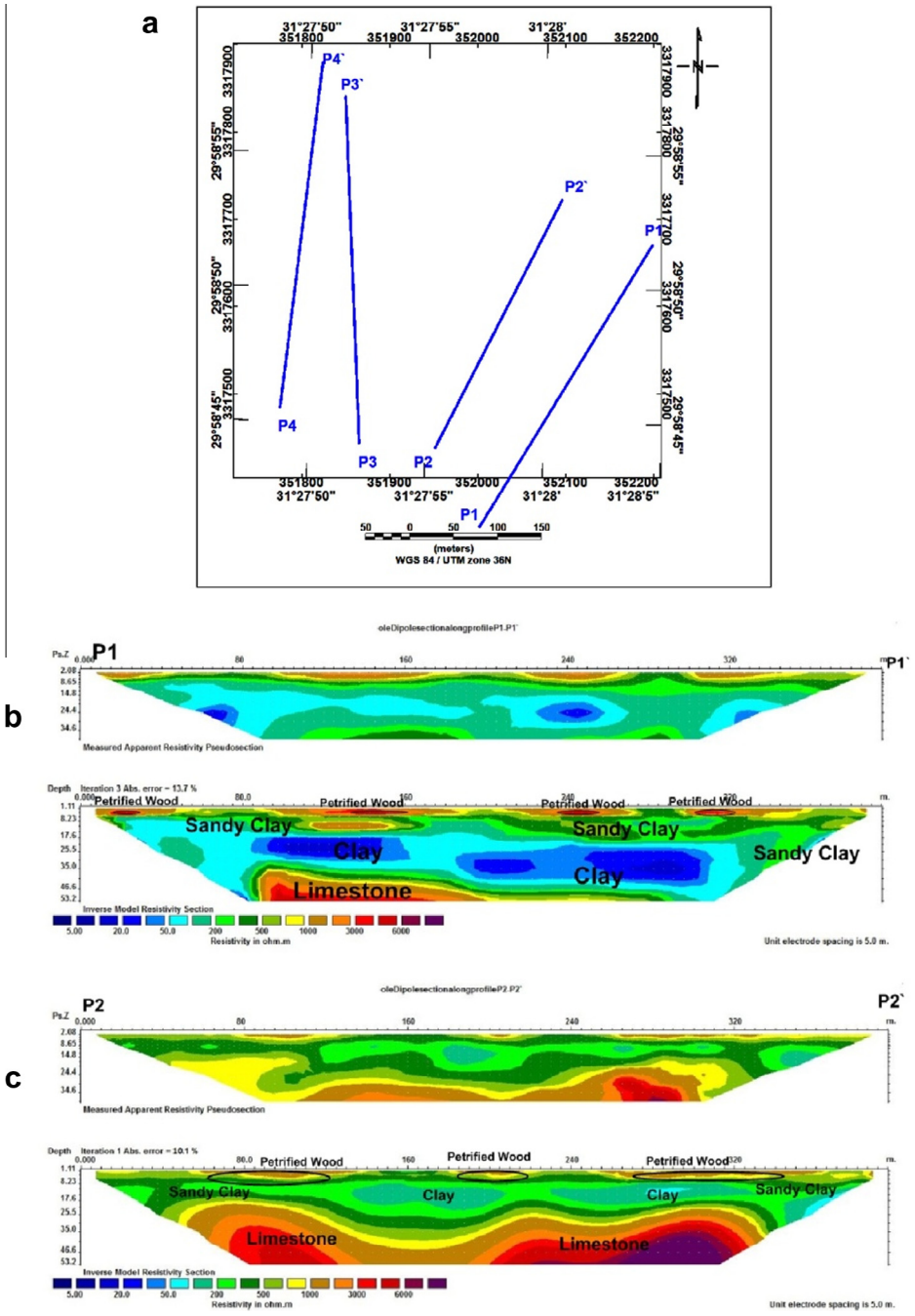

Figure 11 (a) Location map of the dipole–dipole sections and seismic profiles (P1–P3), P4 only for dipole–dipole section. (b) ERT section of dipole–dipole array along profile P1–P1′, (c) ERT section of dipole–dipole array along profile P2–P2′.

three to five times the maximum depth anticipated [18]. Five shots are carried out as follows; the first shot is the normal one at the first geophone; the second shot at the half distance between geophones 6–7; the third one is the midpoint between the geophones 12 and 13; the fourth one between geophones 17–18; the last shot is the reverse one at the last geophone (geophone 24). The Seismic refraction data are interpreted using SeisImager software packages [19]. The picked first-arrival times are inverted in the corresponding depth–velocity section using the reciprocal method [20]. Seismic refraction data interpretation is usually used for depth determination under the shot point and beneath each geophone and also for the calculation of the true velocities for each investigation layer. Interpretation methods based on delay time, plus-minus, generalized reciprocal time and ray-tracing are well explained in the literature, [21–24]. The depth section of seismic refraction profiles (Figs. 13–15) shows three main seismic layers; the uppermost layer is a thin surface layer that extends to a depth of a few meters, and is characterized by low velocity ranging from 462 to 583 m/s corresponding to sand, gravel and Petrified wood. The second seismic layer has a velocity ranging from 1892 to 2192 m/s which is corresponding to

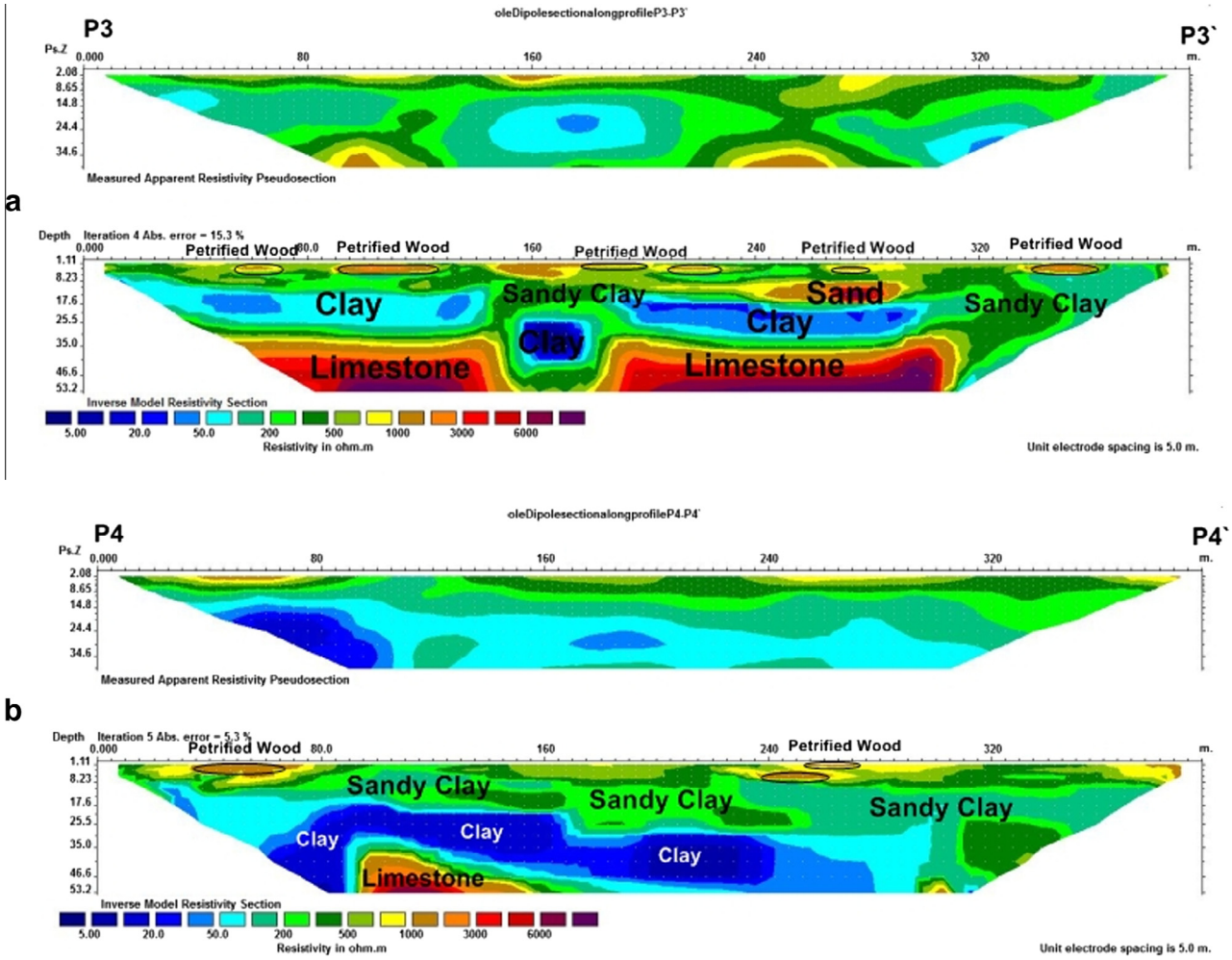

Figure 12 (a) ERT section of dipole–dipole array along a profile P3–P3′, (b) ERT section of dipole–dipole array along profile P4–P4′.

sandy clay and clay of average thickness about 22 m and the seismic layer which is the bedrock (limestone) reflects a high seismic velocity about 4000 m/s.

4. Discussion and conclusion

The field observation of the study area shows that the Petrified wood traced in the southern part of the regional area, where the result of geoelectric and geoseismic section indicates that the trend of the Petrified wood is matched with field observations and these trends of Petrified wood extended to the depth of a few meters. The Petrified wood was transported from the place of growth by running water and buried in the shallow depths. The trends of fault elements are concerned with the trends of Petrified wood, and this may be the answer to the puzzling question about silicification of wood and the role of faults in petrification processes. Also, the Petrified wood exhibits high velocity and resistivity values which can be distinguished from the trends of Petrified wood. The locations of Petrified wood reflect a low magnetic anomaly which indicates about this a part of the area is a basin.

From the integrated interpretation of the geologic, magnetic, electric resistivity and seismic data, we can conclude that the study area is dissected by different fault elements of directions NE–SW, NW–SE, N–S and E–W trends. The southeastern part of the study area which represents the detailed area reveals low magnetic anomaly indicating the basin and the Petrified wood accumulated in it. The subsurface stratigraphy consists of four layers, the first layer is characterized by high resistivity values up to 1000 ohm m corresponding to sand, gravel and Petrified wood at the surface and extends to a depth of a few meters. The second layer is corresponding to sandy clay which exhibits moderate resistivity values of thickness ranging from 6 to 10 m. The third layer is characterized by very low resistivity corresponding to clay of depth ranging from 10 to 30 m overlaying the fourth unit which is characterized by very high resistivity (8000 ohm m) corresponding to limestone. The interpretation of electric resistivity data confirmed the seismic data, where there are three main seismic layers and the uppermost layer is a thin surface layer that extends to a depth of a few meters, and is characterized by low velocity ranging from 462 to 583 m/s corresponding to sand & gravel and Petrified wood. The second seismic layer has a velocity ranging from 1892 to 2192 m/s which corresponds to sandy clay and clay of average thickness of about 22 m and the seismic layer which is the bedrock (limestone) reflects a high seismic velocity of about 4000 m/s.

Please cite this article in press as: S.A.S. Araffa et al., Contribution of geophysical studies on detection of the Petrified Frost Qattamiya, Cairo, Egypt, Egypt. J. Petrol. (2016), http://dx.doi.org/10.1016/j.ejpe.2015.12.003

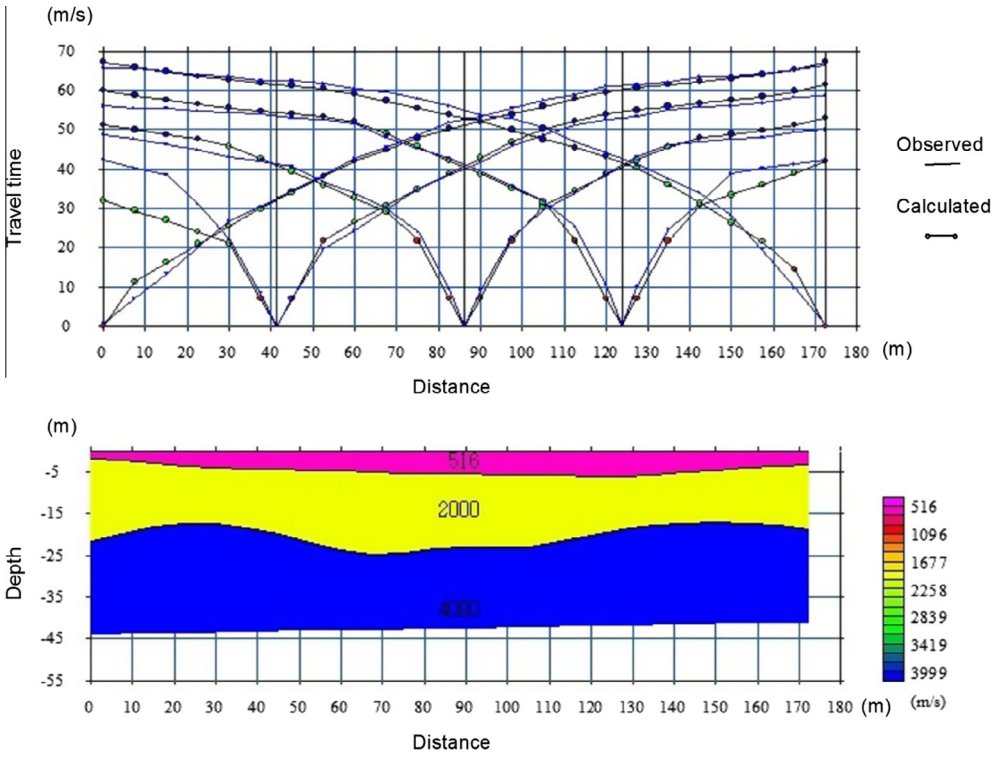

Figure 13 Travel time and corresponding velocity depth section of seismic refraction profiles(1).

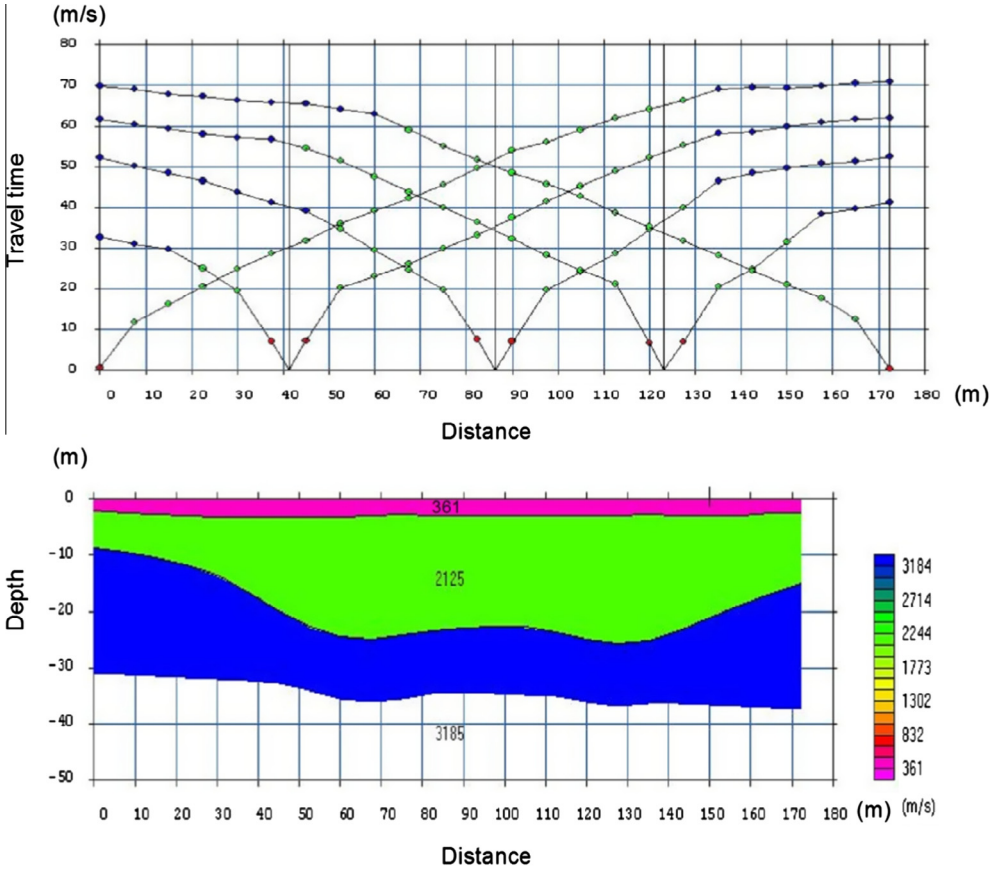

Figure 14 Travel time and corresponding velocity depth section of seismic refraction profiles(2).

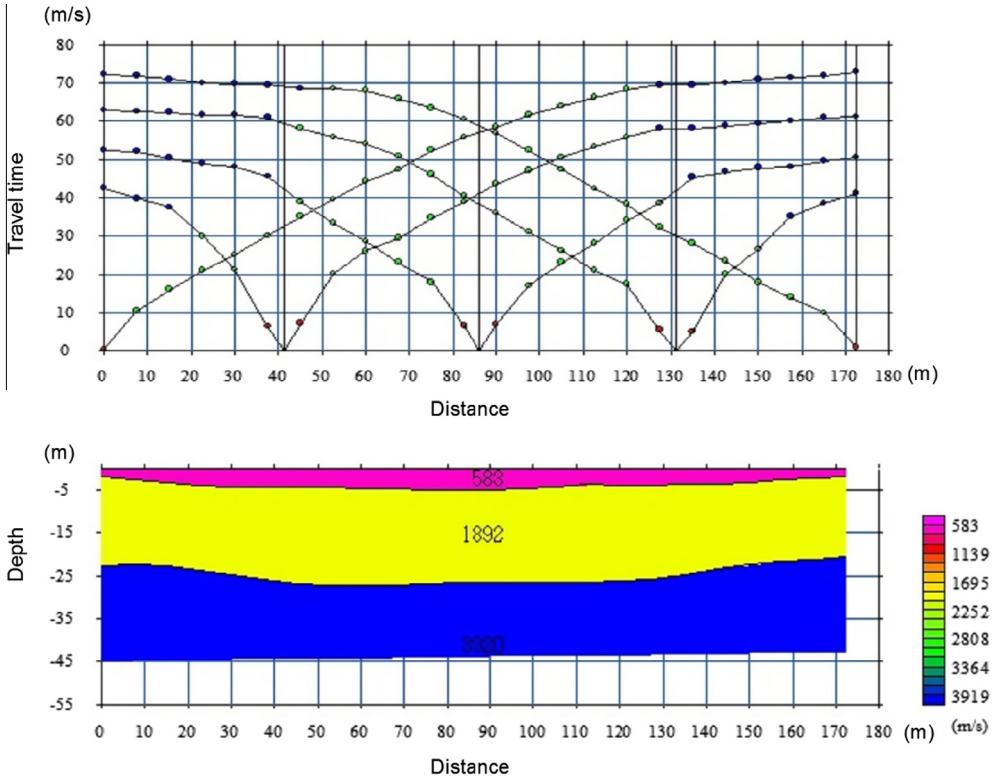

Figure 15 Travel time and corresponding velocity depth section of seismic refraction profiles(3).

References

[1] A.M. Salama, Genesis, Composition and Geological Significance of wood fossils in Maadi Qattamiya Area (M.Sc. Thesis), Fac., Sci., Cairo Univ. p. 118, 2008.
[2] W. El-Saadawi, M.M. Kamal-El-Din, AttiaYusri, M.W. El.-Faramawi, Rev. Palaeobot. Palynol. 167 (3) (2011) 184–195.
[3] G. Vargemezis, N. Diamanti, P. Tsourlos, I. Fikos, Electrical Resistivity Tomography and Ground Penetrating Radar for locating buried petrified wood sites: a case study in the natural monument of the Petrified Forest of Evros, Greece, Geophysical Research Abstracts, vol. 16, EGU2014-14298, EGU General Assembly, 2014.
[4] J.W. Martz, W.G. Parker, L. Skinner, J.J. Raucci, P. Umhoefer, R.C. Blakey, Geologic Map of Petrified Forest National Park, Arizona, Geological survey of Arizona, Contributed Report CM-12-A, pp. 1–17, 2012.
[5] A.M.E. Mohamed, S.A. Sultan, N.I. Mahmoud, Pure Appl. Geophys. 169 (2012) 1641–1654.
[6] S.A.S. Araffa, Environmental Earth Sci. J. 59 (2010) 1195–2207.
[7] S.A.S. Araffa, Int. J. Geophys. 192 (1) (2013) 94–112.
[8] S.A.S. Araffa, F.A. Monteiro Santos, T.A. Hamed, Environ Earth Sci. 71 (2014) 3293–3305.
[9] R. Said, The Geology of Egypt, Elsevier Publication, 1962, p. 377.
[10] R. Said, The Geology of Egypt, Balkema, 1990, p. 734.
[11] H. Akahane, T. Furuno, H. Miyajima, T. Yoshikawa, S. Yamamoto, Sed. Geol. 169 (2004) 219–228.
[12] Oasis Montaj, Geosoft mapping and application system Inc, Suit 500, Richmond St. West Toronto, ON Canada N5SIV6, 2007.
[13] V. Baranov, Geophysics 22 (1957) 359–383.
[14] V. Baranov, H. Naudy, Geophysics 29 (1964) 67–79.
[15] V. Baranov, Potential fields and their transformation in applied geophysics. Geoexploration Monographs, series 1–6, Gebrüder, Borntraeger, Berlin – Stuttgart, 1975.
[16] D.T. Thompson, Geophysics 47 (1) (1982) 31–37.
[17] M.H. Loke, R.D. Barker, Geophys. Prospect. 44 (1996) 131–152.
[18] B.B. Redpath, Seismic Refraction Exploration for Engineering Site Investigations, Technical Report E-73-4, U.S., Army Engineering Waterways Experiment Station Explosive Excavation Research Laboratory, Livermore, California, 1973.
[19] SeisImager, Windows Software Package for Analysis of Surface Waves, Ver. 3.0, Geometrics Inc., 2008.
[20] Palmer,, Refraction seismic, in: K. Helbig, S. Treitel (Eds.), Vol. 13, Geophysical Press, London, 1986.
[21] X. Zhu, G. McMechan, Ray Tracing for Surface Source-to-surface Recorder Tomography, Center for Lithospheric Studies, University of Texas, Dallas, 1988.
[22] D. Palmer, Exp. Geophys. 31 (2000) 275–280.
[23] D. Palmer, The shallow refraction method for the new millennium Website, Dr. Derecke Palmer htm, Science@UNSW, 2003.
[24] D. Palmer, L. Jones, Detailed refraction statics with the GRM and RCS, ASEG 16th Geophysical Conference and Exhibition, Adelaide, Expanded Abstracts, 2003.